JGR Atmospheres

RESEARCH ARTICLE
10.1029/2022JD036734

Special Section:
Fire in the Earth System

Contribution of Fire Emissions to $PM_{2.5}$ and Its Transport Mechanism Over the Yungui Plateau, China During 2015–2019

Jun Zhu[1], Xu Yue[1], Huizheng Che[2], Xiangao Xia[3,4], Yadong Lei[2], Jun Wang[5], Tianliang Zhao[6], Xingna Yu[6], Hao Zhou[4,7], and Hong Liao[1]

[1]Jiangsu Key Laboratory of Atmospheric Environment Monitoring and Pollution Control, Collaborative Innovation Center of Atmospheric Environment and Equipment Technology, School of Environmental Science and Engineering, Nanjing University of Information Science & Technology (NUIST), Nanjing, China, [2]State Key Laboratory of Severe Weather (LASW) and Key Laboratory of Atmospheric Chemistry (LAC), Chinese Academy of Meteorological Sciences, CMA, Beijing, China, [3]LAGEO, Institute of Atmospheric Physics, Chinese Academy of Sciences, Beijing, China, [4]University of Chinese Academy of Sciences, Beijing, China, [5]Center of Global and Regional Environmental Research and Department of Chemical and Biochemical Engineering, University of Iowa, Iowa, IA, USA, [6]Key Laboratory for Aerosol-Cloud-Precipitation of China Meteorological Administration, Nanjing University of Information Science and Technology, Nanjing, China, [7]Climate Change Research Center, Institute of Atmospheric Physics (IAP), Chinese Academy of Sciences (CAS), Beijing, China

Key Points:

- Average $PM_{2.5}$ concentrations at Yungui Plateau (YGP) stations were 36.06 ± 14.86 μg m^{-3} with the highest value at the nearest station to the Indo-China Peninsula
- Fire emissions contributed $50\% \pm 20\%$ of the vertical $PM_{2.5}$ at a height of 3–4 km over the YGP
- Four weather patterns with low air pressure were favorable for the transport of $PM_{2.5}$ to the YGP through two typical pathways

Correspondence to:
X. Yue,
yuexu@nuist.edu.cn

Citation:
Zhu, J., Yue, X., Che, H., Xia, X., Lei, Y., Wang, J., et al. (2022). Contribution of fire emissions to $PM_{2.5}$ and its transport mechanism over the Yungui Plateau, China during 2015–2019. *Journal of Geophysical Research: Atmospheres*, *127*, e2022JD036734. https://doi.org/10.1029/2022JD036734

Received 8 MAR 2022
Accepted 12 JUN 2022

Author Contributions:
Conceptualization: Jun Zhu, Xu Yue
Data curation: Huizheng Che, Yadong Lei
Formal analysis: Jun Zhu, Yadong Lei
Investigation: Jun Zhu, Xu Yue
Validation: Xiangao Xia
Writing – original draft: Jun Zhu
Writing – review & editing: Xu Yue, Huizheng Che, Xiangao Xia, Jun Wang, Tianliang Zhao, Xingna Yu, Hao Zhou, Hong Liao

Abstract Air pollution over the Yungui Plateau (YGP) in southwestern China can be caused by the transport of biomass burning aerosols from Southeast Asia; however, the magnitude and mechanisms of such long-range transport have not been fully investigated. Here, we studied the impacts of fire emissions on vertical $PM_{2.5}$ over the YGP and the transport mechanisms of $PM_{2.5}$ during the fire seasons (March–April) of the neighboring Indo-China Peninsula (ICP) region in 2015–2019 using ground-based monitoring data, reanalysis of meteorology, and GEOS-Chem model simulations. Average daily $PM_{2.5}$ concentrations of 36.06 ± 14.86 μg m^{-3} were measured at 16 ground stations in the YGP with the highest value of 53.77 μg m^{-3} at Xishuangbanna, the nearest station to the ICP. Model simulations showed that fire emissions contributed approximately 50%–60% of the vertical $PM_{2.5}$ over the YGP at a height of 3–4 km, with larger contributions in meridional than zonal cross-sections. Four weather patterns with low pressure over the YGP were identified as favorable conditions for smoke transport. The pattern with the lowest pressure over the northern YGP and the strongest vertical wind disturbance was the most favorable for the eastward transport of fire air pollution to the YGP. Another pattern, which had the strongest southerly wind, promoted smoke aerosols to climb from eastern Myanmar and northern Laos/Vietnam to the YGP. Through these typical pathways, ICP biomass burning significantly impacted $PM_{2.5}$ pollution in southwestern China.

Plain Language Summary Based on the ground atmospheric monitoring data, reanalysis of meteorological data, and simulations of chemical transport model, we studied the impacts of fire emissions on vertical $PM_{2.5}$ over the Yungui Plateau (YGP) and the transport mechanisms of $PM_{2.5}$ during the fire season of the neighboring Indo-China Peninsula (ICP) region in 2015–2019. We find that fire emissions contributed approximately 50%{plus minus}20% of the vertical $PM_{2.5}$ over the YGP at a height of 3–4 km, with larger contributions in meridional than zonal cross-sections. Four weather patterns with low pressure over the YGP were identified as favorable conditions for smoke transport and the weather pattern showed two typical pathways of smoke transport from the ICP to the YGP. This study reveals the large impacts of trans-boundary air pollution from the ICP on the air quality in the YGP during biomass burning seasons.

1. Introduction

The heavy haze that has occurred in recent years in China has been largely attributed to atmospheric aerosols (Zhang et al., 2015), especially fine particulate matter with an aerodynamic diameter less than 2.5 μm ($PM_{2.5}$). These small particles can affect the climate through aerosol–radiation and aerosol–cloud interactions (Huang et al., 2006; Li et al., 2017a; Liu et al., 2011; Takemura et al., 2005; Yang et al., 2017). The concentrations and composition of $PM_{2.5}$ show large spatiotemporal variability owing to their complex formation and transport processes, leading to large uncertainties in the estimation of aerosol impacts on the environment and climate (IPCC, 2013).

Although $PM_{2.5}$ in China is mainly attributed to anthropogenic emissions (Zhang & Cao, 2015; Zhang et al., 2019), natural emissions, such as biomass burning, play an important role in modulating regional air quality. Previous studies have estimated annual $PM_{2.5}$ emissions of 3,526.7 Gg from biomass burning in China (Zhou et al., 2017). During the fire season, the contribution of biomass burning to $PM_{2.5}$ can reach 11% in Beijing (Song et al., 2006), 37% in the Yangtze River Delta (Cheng et al., 2014), and 19% in the Pearl River Delta (Cheng et al., 2014; Wang et al., 2007). $PM_{2.5}$ that is emitted by intense burning affects not only local air but also that of downwind regions through atmospheric transport (Li et al., 2019, 2021; Poulain et al., 2021; Wang et al., 2018). The impact of smoke transport has been well studied in regions with frequent fire activities, such as Central America (Saide et al., 2015; Wang & Christopher, 2006), Russia (Li et al., 2019; Mielonen et al., 2012; Péré et al., 2014), Africa (Ansmann et al., 2009; Williams et al., 2012), and South/Southeast Asia (Ding et al., 2021; Engling et al., 2011; Wang et al., 2017, 2021; Zhang et al., 2018; Zhu et al., 2019).

The Yungui Plateau (YGP), located in southwestern China, experiences cross-boundary transport of air pollutants from fire emissions in Southeast Asia every spring (Dong & Fu, 2015; Liang et al., 2019). The elevation of the YGP is generally greater than 2,000 m, with mountain peaks as high as 3,700 m. The annual aerosol loading over the YGP is relatively low with an aerosol optical depth (AOD) of 0.1–0.2 (Li et al., 2003; Luo et al., 2014), but the surrounding regions show high AOD levels with frequent biomass burning in the Indo-China Peninsula (ICP) during the late dry season (Streets et al., 2003). Previous studies have revealed the significant impacts of biomass burning in the ICP on aerosols over the YGP region. For example, Zhu et al. (2017) indicated that biomass burning from Southeast Asia contributed to approximately 57% of the total AOD over the city of Kunming in the YGP during March and April from 2012 to 2013. In a case study, Xing et al. (2021) reported that biomass burning from Southeast Asia increased $PM_{2.5}$ concentrations in Yunnan Province by 39.3 μg m^{-3} (68.0%). In another case, Li et al. (2017b) showed that fires in the ICP contributed 10%–40% of the near-surface $PM_{2.5}$ in southwestern China. However, most of these studies explored fire contributions based on 1–2 cases or for short periods. The transport mechanisms and long-term impacts of biomass burning on the YGP have not been fully investigated, especially for vertical transport above a high altitude of >2 km.

In this study, we explored the multi-year impacts of biomass burning on vertical $PM_{2.5}$ using both observations and model simulations. We specially focused on the transport processes of aerosols from the ICP region to the YGP during the fire season. Section 2 describes the observational stations, data, and methods. Section 3 explores the spatiotemporal variations in $PM_{2.5}$, the impacts of biomass burning on vertical $PM_{2.5}$, and the potential weather patterns and vertical transport mechanism of aerosols from the ICP region to the YGP.

2. Data and Methodology

2.1. Ground-Based Stations and $PM_{2.5}$ Data

In this study, 16 ground-based stations from China's Ministry of Ecology and Environment in Yunnan Province of the YGP were used. Every station included 2–3 observational sites, and the values of all sites in a station were averaged to represent the station. Figure 1 shows the topography of the study region (YGP and ICP) and 16 ground-based stations located in Yunnan in the YGP. The 16 stations in the study area were divided into four groups: northwest (NW), northeast (NE), southwest (SW), and southeast (SE), with 3–5 stations in each group. The dividing lines were latitude 24.5°N and longitude 101.25°E, which were selected based on a comprehensive consideration of the distribution of stations, potential pathways of smoke transport from the ICP to the YGP, and resolution of the model simulation. In the YGP and ICP, the mean climate showed apparent rainy (May–October) and dry (November–April) seasons that were associated with monsoon onsets in May and withdrawals in October (Yan et al., 2013). Since biomass burning events occurred more frequently in the late dry season (which was also the transition period from dry to wet) in Southeast Asia, this work focused only on the late dry season (March–April, which was also the biomass burning period).

The $PM_{2.5}$ concentrations are measured using the micro oscillating balance method and/or the β absorption method from commercial instruments. The instrumental operation, maintenance, data assurance and quality control are properly conducted according to the China Environmental Protection Standards revised in 2013 (Zhang & Cao, 2015). Past studies have showed that the data from the China's Ministry of Ecology and Environment stations fit the Benford's Law and were highly consistent with the data measured by U.S. Embassy in china

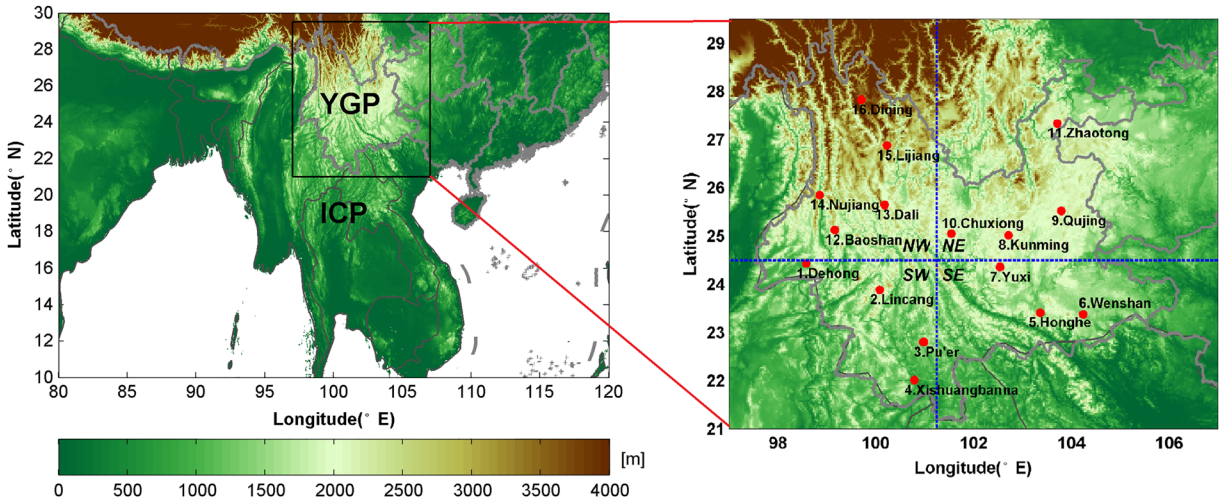

Figure 1. Topography of the study area and the 16 ground-based stations located at the Yungui Plateau (YGP), which are separated into four regions: northwest (NW), northeast (NE), southwest (SW), and southeast (SE). The neighboring Indo-China Peninsula (ICP) region is shown in the left panel.

with correlations of >95% at most cities since 2013 (Liang et al., 2016; Stoerk, 2016). The hourly concentrations of $PM_{2.5}$ at the 16 stations in the YGP region during the late dry season from 2015 to 2019 were collected.

2.2. Global Fire Emissions Database (GFED)

The Global Fire Emissions Database (GFED) version 4.1 (GFED4s) (van der Werf et al., 2017) was analyzed and used as a biomass burning inventory for simulations. The GFED derives biomass burned based on satellite retrieval of burned areas and active fire information (Giglio et al., 2013). GFED4s considers six land cover types: temperate forests, peat, savanna, deforestation, boreal forest, and agricultural waste. For each land type, fire-induced emissions were estimated as the product of the dry matter and species-specific emission factors from Akagi et al. (2011). By default, GFED4s provides monthly fire emissions with a spatial resolution of 0.25° from 1997 to the present (December 2021). Since 2003, daily fire emissions data have been available by multiplying daily scale factors with monthly emissions data (Mu et al., 2011).

2.3. ERA5 Reanalysis Meteorological Data

The European Center for Medium-Range Weather Forecasts (ECMWF) produces global numerical weather predictions for members and cooperating states and reanalysis data for a broader community (Hoffmann et al., 2019). The fifth-generation ECMWF atmospheric reanalysis system (ERA5) provides hourly wind fields on a 0.25° × 0.25° latitude/longitude grid (Hersbach et al., 2020). The 800 hPa wind field and geopotential height were used to classify the weather pattern on regional pollution days following the *k*-means classification method proposed by Lloyd (1982). Three-dimensional wind fields, including zonal u, meridional v, and vertical velocity w, were used to study the dynamic conditions of transportation.

2.4. GEOS-Chem Simulations

2.4.1. GEOS-Chem Model and Configuration

The 3-D GEOS-Chem (http://wiki.seas.harvard.edu/geos-chem/) chemical transport model version 12.0.0, with 2° × 2.5° horizontal resolution and 47 layers from the surface to 0.01 hPa for the vertical grid (Bey et al., 2001), was used to estimate fire-induced $PM_{2.5}$. The model was driven by the Global Modeling and Assimilation Office MERRA-2 meteorology, with a temporal resolution of 3 hr for meteorological parameters and 1 hr for surface fields. The model included a fully coupled O_3-NOx-hydrocarbon-aerosol chemical mechanism to simulate the atmospheric composition and air quality (Gong & Liao, 2019; Lei et al., 2020). All GEOS-Chem emissions were configured at runtime using the Harvard–NASA Emission Component module described by Keller

et al. (2014). The default global anthropogenic emissions were overwritten over East Asia by the MIX inventory of Li et al. (2017c). The biomass burning inventory was adopted from GFED4s. GEOS-Chem used the TPCORE advection algorithm proposed by Lin and Rood (1996). Convective transport was computed from convective mass fluxes in the meteorological fields, as described by Wu et al. (2007). The boundary layer mixing in GEOS-Chem used the nonlocal scheme implemented by Lin and McElroy (2010). Dry deposition was based on Wesely (1989), as implemented by Wang et al. (1998), and aerosol deposition was based on Zhang et al. (2001). Wet deposition was performed as previously described by Liu et al. (2001). Studies have shown that GEOS-Chem captures the spatiotemporal variability of $PM_{2.5}$ in China (Dang & Liao, 2019).

2.4.2. Model Experiment Design

We performed full-chemistry simulation that included fire emissions from March 2015 to April 2019 with 2 months of spin-up. The $PM_{2.5}$ output diagnosis was set to three dimensions and a daily average, which was used to show the three-dimensional characteristics of $PM_{2.5}$ during the pollution period of the YGP. We also conducted a sensitivity simulation without fire emissions, which was used to explore the contributions of fire to $PM_{2.5}$. We used "Fire" and "Nofire" to represent the model simulations with and without fire emissions, respectively.

2.5. Classification of Weather Patterns

We classified the weather patterns adopting the k-means classification method proposed by Lloyd (1982). Considering the height and range of the plateau, the geopotential height at 800 hPa and the domain (10–30°N, 90–110°E) covered YGP on the days of regional air pollution were chosen to represent the synoptic patterns. Through calculation, there were 33 days of regional air pollution due to $PM_{2.5}$ in YGP which was shown in next section. The steps of the classification method are as followed. Step 1, choose k (predefined number of patterns) initial cluster centers (centroid) among the 33 days. Here use the k-means ++ algorithm for cluster center initialization (Arthur & Vassilvitskii, 2006). Step 2, compute the correlations between the daily geopotential height with location information on all pollution days to each centroid. Step 3, assign each pollution day to the cluster with the closest centroid (the largest correction). Step 4, compute the average of the days in each cluster to obtain k new centroid locations. Step 5, repeat steps 2 through four until cluster assignments do not change, or the maximum number of iterations (100) is reached. We selected the numbers of clusters (2–8) to classification, and then used elbow method (the corner of the Sum Square Error) to determine the last number of clusters (=4 in this study).

3. Results and Discussion

3.1. Variations in Ground-Based $PM_{2.5}$ Over the YGP During the Late Dry Season

Figure 2a shows the daily $PM_{2.5}$ concentrations of the 16 stations in the YGP during the late dry season from 2015 to 2019. The SW and SE regions in the YGP showed high $PM_{2.5}$ concentrations, with regional averages larger than 40 μg m^{-3}, while the NE and NW regions had averages less than 40 μg m^{-3}. The regional order of the mean daily $PM_{2.5}$ concentrations was SW > SE > NE > NW, indicating that the southern area of the YGP suffered more aerosol pollution than the northern area. Among these stations, the southernmost station Xishuangbanna experienced the highest mean $PM_{2.5}$ concentrations (53.77 ± 26.23 μg m^{-3}). In contrast, Lijiang (14.52 ± 5.74 μg m^{-3}) and Diqing (14.52 ± 3.83 μg m^{-3}), stations far from the ICP at high altitudes of 3,000 m, showed the lowest $PM_{2.5}$ concentrations. The average $PM_{2.5}$ concentrations for all 16 stations at YGP in the study period was 36.06 ± 14.86 μg m^{-3}, lower than the mean $PM_{2.5}$ concentrations of 78 in the North China Plain and >40 μg m^{-3} in the Yangtze River Delta (Hu et al., 2014; Li et al., 2020; Ming et al., 2017).

According to the China National Ambient Air Quality Standards for $PM_{2.5}$ in 2012 (GB3095–2012), we calculated the frequency of $PM_{2.5}$ at different levels during March–April of 2015–2019 (Figure 2b). The frequency of $PM_{2.5}$ on most days at all YGP stations was below the pollution standard (75 μg m^{-3}). The SW and SE stations (except for Yuxi Station) showed the highest percentage (52.13%–71.80%) of days at a good level, while the NW and NE stations (except for Kunming Station) showed the highest percentage (54.43%–100%) of days at an excellent level. However, most stations had days when daily $PM_{2.5}$ reached the polluted level (daily $PM_{2.5}$ > 75 μg m^{-3}). Some stations (all SW stations and two stations in the NW region) even experienced medium pollution (75 < daily $PM_{2.5}$ < 115 μg m^{-3}). Only Xishuangbanna Station showed severe pollution for 1 day (daily $PM_{2.5}$ > 150 μg m^{-3}). The percentages of daily $PM_{2.5}$ above the polluted level during March–April of 2015–2019 were 6.56%–18.69%

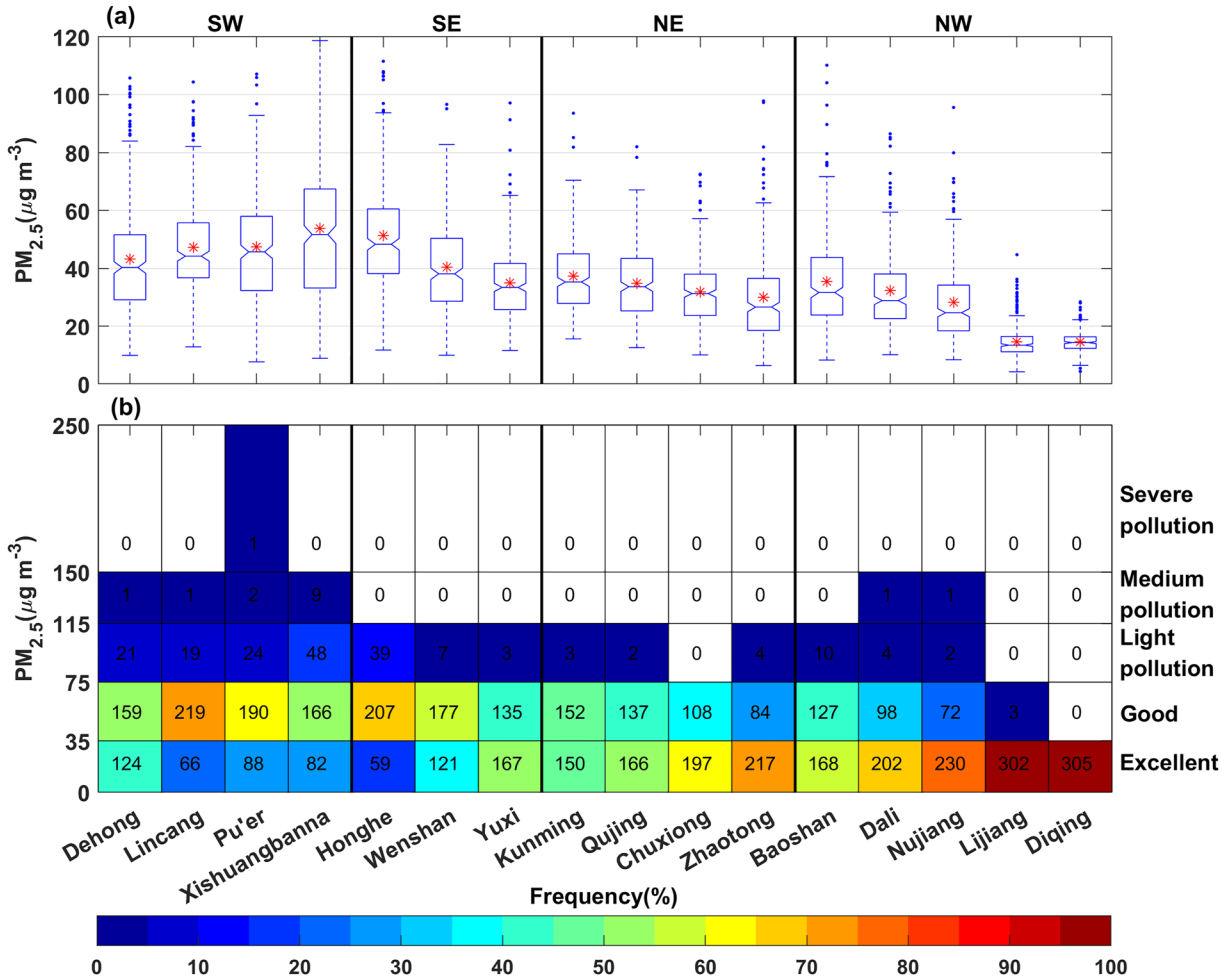

Figure 2. Statistics of daily $PM_{2.5}$ concentrations of the 16 sites over the Yungui Plateau during March–April from 2015 to 2019. (a) Box plots. In each box, the central bar is the median and the lower and upper limits are the first and the third quartiles, respectively. The lines extending vertically from the box indicate the spread of the distribution with the length being 1.5 times the difference between the first and the third quartiles. The asterisk symbols indicate geometric means. (b) Frequency distribution. The values in grids are the number of days for corresponding thresholds of $PM_{2.5}$ concentrations.

for the SW stations and 0.98%–12.79% for the SE stations. Such ratios were much higher than the annual mean frequency of 1.84% for Yunnan for polluted level, suggesting that the late dry season (March–April) was a typical pollution period for the YGP.

To explore the impact of smoke transport on $PM_{2.5}$ over YGP, we identified regional pollution events with multiple stations experiencing air pollution on the same days. For each region in the YGP, a polluted day was defined as when more than half of the stations within the region were polluted. Figure 3 shows the polluted days for stations and regions during March–April in 2015–2019. There were 30, 7, 1, and 1 day with daily $PM_{2.5}$ reaching pollution levels in the SW, SE, NE, and NW regions, respectively. The SW region showed the most polluted days, and its periods of pollution often coincided with the other three regions, suggesting the possible transport of air pollution through SW to other regions (Li et al., 2017b). In total, there were 33 days of regional pollution during March–April in 2015–2019, with a relatively low number of polluted days in 2016 and 2018.

3.2. Contribution of Fire Emissions to $PM_{2.5}$ Concentrations

We used the GEOS-Chem model to quantify the contributions of fire emissions to the $PM_{2.5}$ concentrations over the YGP during March–April in 2015–2019. Evaluations showed that the model reasonably captured the spatial distribution of $PM_{2.5}$ with high levels of $PM_{2.5}$ in the south and SW and low levels of $PM_{2.5}$ in the north and NE of the YGP (Figure 4a). For a total of 528 samples across stations and days, the model predictions yielded a

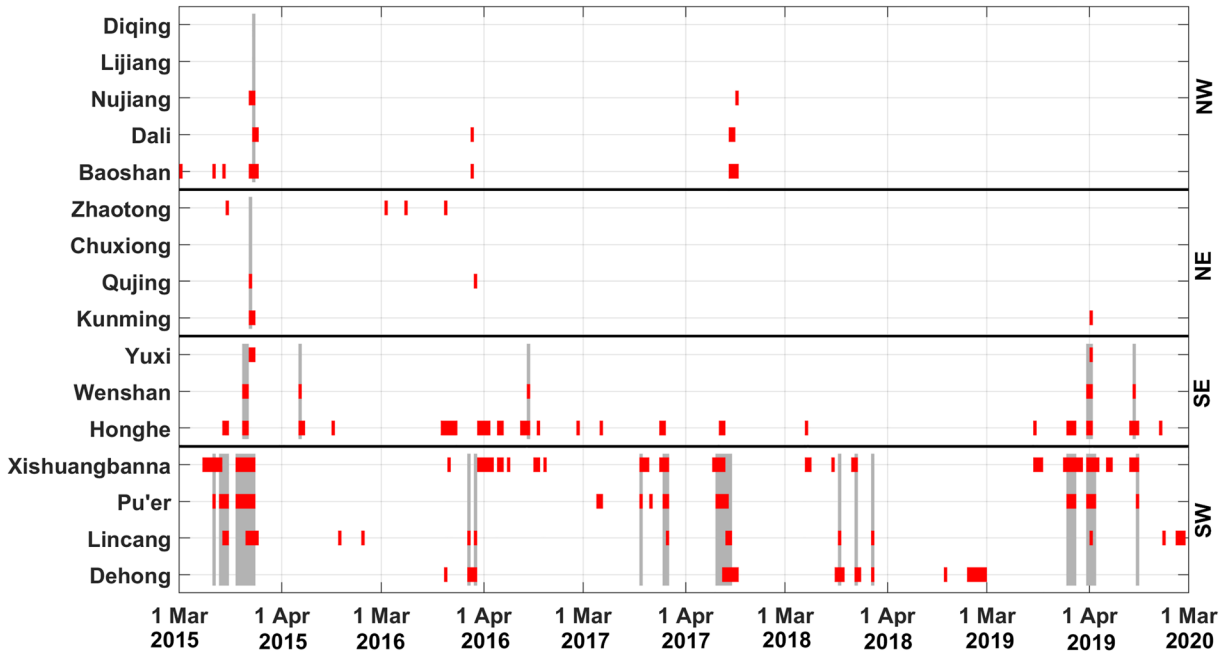

Figure 3. The polluted day at each site (red) and for each region (gray) during March–April from 2015 to 2019.

good correlation coefficient of 0.53 (Figure 4b), suggesting that the simulations in general reproduced observed spatiotemporal variations of $PM_{2.5}$ concentrations over the YGP on regional polluted days during March–April in 2015–2019.

We quantified the absolute (Fire-Nofire) and relative ((Fire-Nofire)/Fire) contributions of fire emissions to vertical $PM_{2.5}$ concentrations in the zonal cross-section which is an average across the latitude of 23–25°N (Figure 5). On average, fire emissions contributed up to 30 μg m^{-3} and 50% of the $PM_{2.5}$ concentrations in the vertical levels. The areas of high contribution ranged from the western to the eastern part of the plateau and showed a tail over the east side of the plateau, indicating a transport pathway of smoke from west to east. Fire contributions

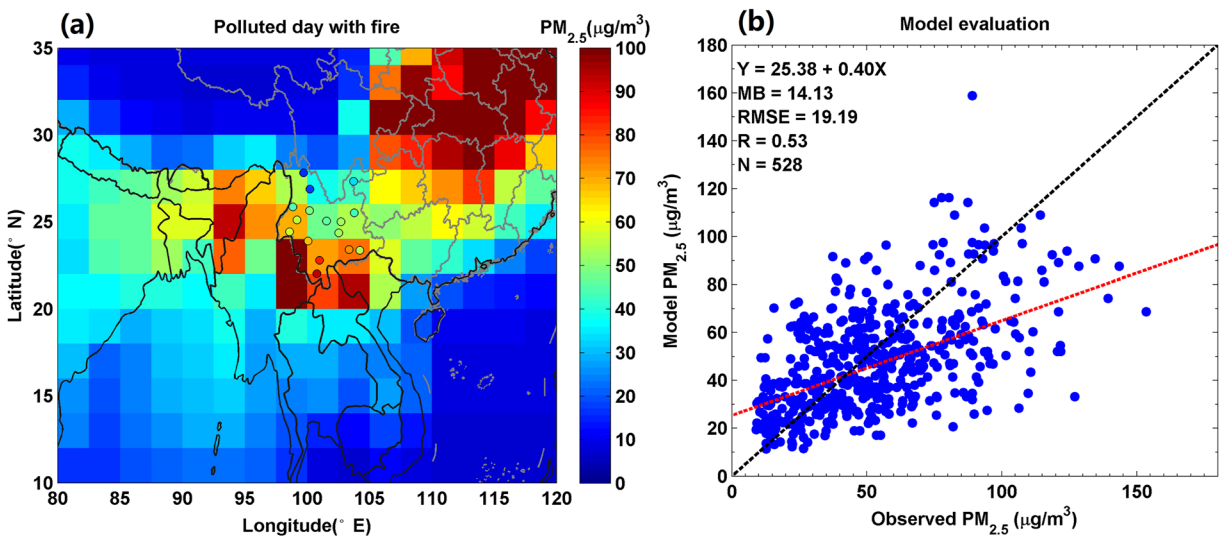

Figure 4. Model evaluation of daily $PM_{2.5}$ concentrations at the surface on regional polluted days by using ground-based observation: (a) special distribution and (b) spatial-temporal matching. The dots with color-filled in (a) are the averages of ground measured daily $PM_{2.5}$ concentrations and the color in each pixel stands for the averaged value of the model simulation on the regional polluted days. The statistical parameters in (b) include the number of matchup data (N), the slope and intercept at the y axis of linear regression (red line), the mean bias (MB), the root-mean-squared error (RMSE), and the correlation coefficient (R).

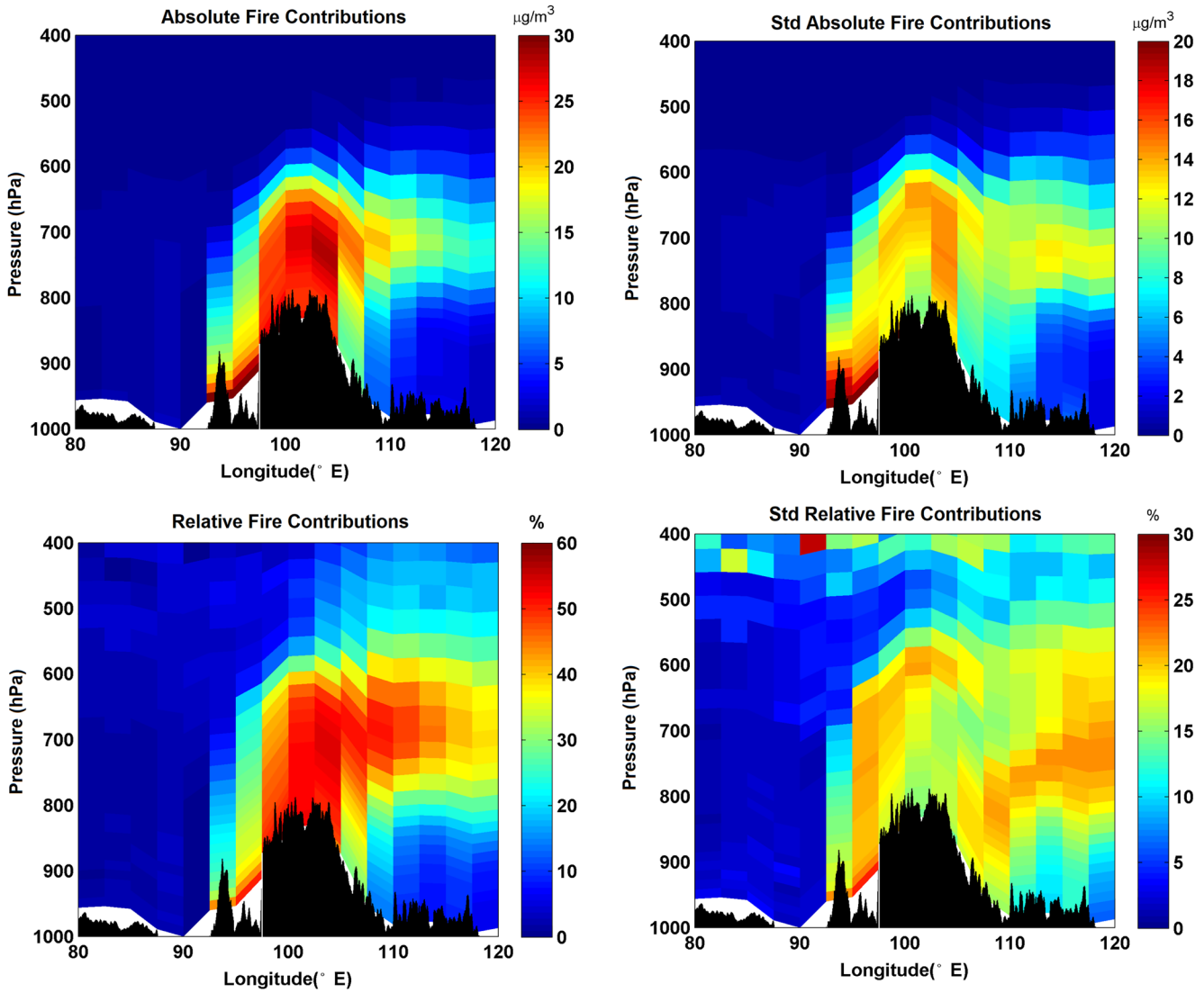

Figure 5. Simulated vertical cross-sections of absolute (Fire-Nofire) and relative ((Fire-Nofire)/Fire) contributions of fire emissions to $PM_{2.5}$ concentrations, and their standard deviations, along the latitude of 24.5°N (showed in Figure 1), averaged for all regional polluted days during March–April in 2015–2019.

are high at the 600 hPa level (~4 km), consistent with the elevated smoke observed by the Cloud-Aerosol Lidar with Orthogonal Polarization over the YGP during spring (Liao et al., 2021). The standard deviations were 10–15 μg m^{-3} for absolute contributions and 15%–23% for relative contributions from the surface to an altitude of approximately 4 km. The meridional vertical cross-section averaged the longitude of 98.75–103.75°E in Figure 6 shows that fire contributions to $PM_{2.5}$ at vertical levels over the YGP could exceed 30 μg m^{-3} (60%), which was higher than that in the zonal cross-section (Figure 5). High fire contributions were near the surface for regions in 20–22°N but extended to 600 hPa (~4 km) for regions in 22–24°N, which is the southern part of the YGP. Fire contributions over the central and northern parts of the YGP (24–28°N) decreased gradually, indicating another smoke transport pathway from south to north.

Our estimated fire contributions of 50 ± 20% to YGP $PM_{2.5}$ were within the range of 10%–70% from previous case studies (Li et al., 2017b; Xing et al., 2021). Such high contributions can extend up to 3–4 km, with a larger magnitude in meridional than zonal cross-section over the YGP.

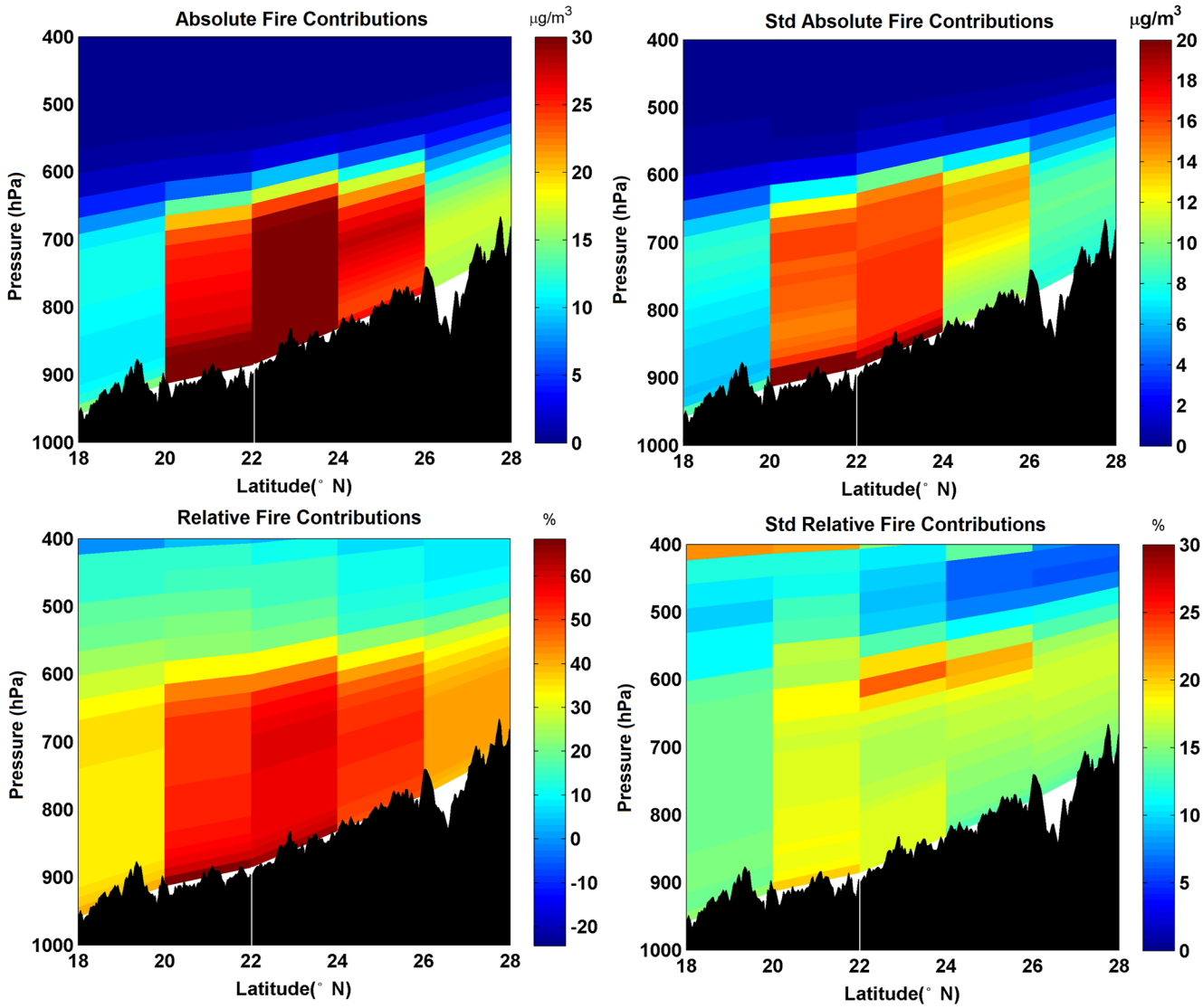

Figure 6. Same as Figure 5 but for the longitude slice of 101.25°E. The white lines represent the approximate boundaries of the Yungui Plateau and Indo-China Peninsula.

3.3. Analyses of Meteorological Conditions

We further explored the sources and transport processes of fire air pollution in the YGP. As shown in Figure 7, fires mainly occurred in the ICP region, adjacent to the south of the YGP. Compared with the ICP, local biomass burning over the YGP was limited. However, southern YGP showed much higher contributions of fire emissions than the northern part (Figure 6), suggesting cross-boundary transport of fire air pollution from the ICP to the YGP. Meteorological conditions play an important role in smoke transport. In this study, we analyzed and identified four major weather patterns during regional pollution days.

Figure 8 shows the mean geopotential height overlaid with horizontal winds at 800 hPa for each of the four weather patterns, which was plotted by averaging all the regional polluted days that belong to that category. The first pattern occurred most frequently, with 17 out of the 33 (51.5%) regional polluted days, followed by Pattern 2 (18.2%), Pattern 4 (18.2%), and Pattern 3 (13.3%). All patterns featured low pressure over the YGP, indicating the regional convergence of the atmosphere. The strength of low pressure decreased gradually from Pattern 1 to 4, with northward placement for Patterns 1–2 and southward placement for Patterns 3–4, leading to more air transport from the west in Patterns 1–2 and from the south in Patterns 3–4. Table 1 shows the statistic of the

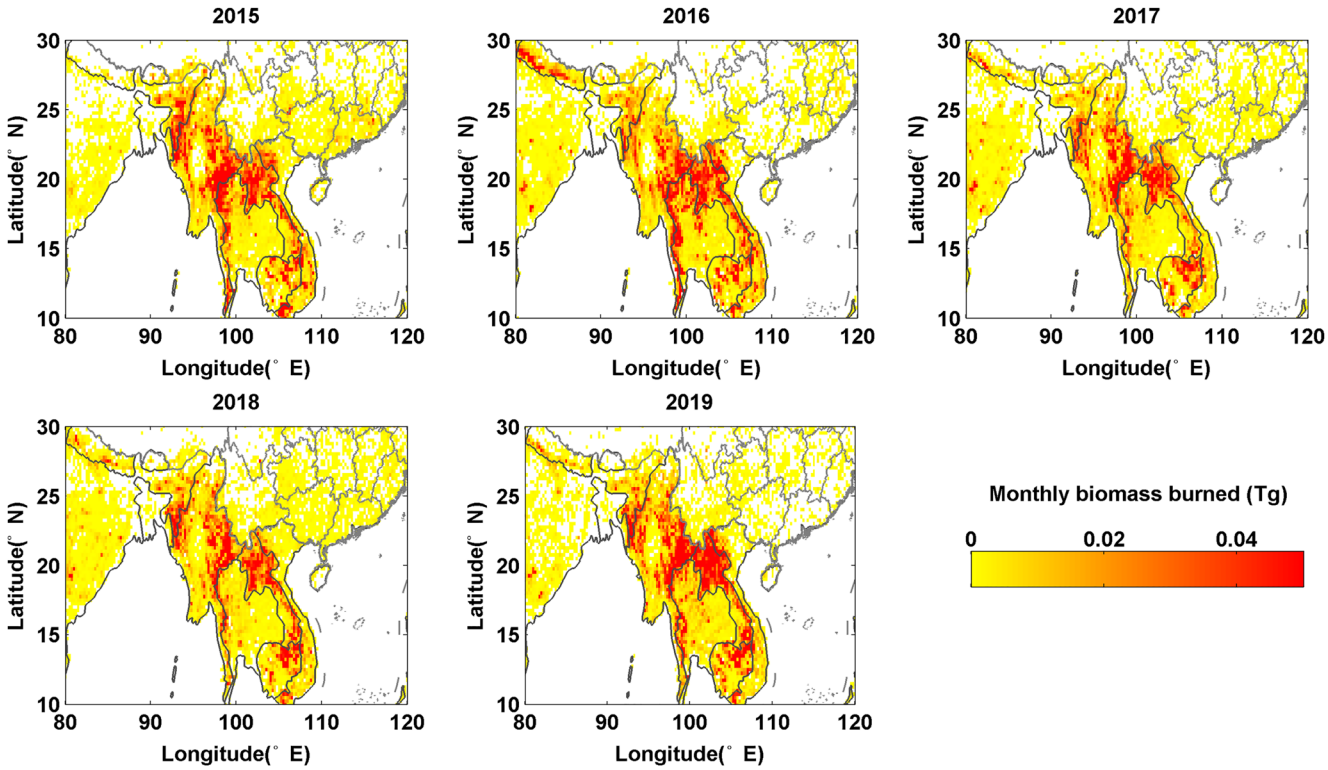

Figure 7. Monthly biomass burned (Tg dry matter) during March–April of 2015–2019 from Global Fire Emissions Database inventory.

mean concentrations of $PM_{2.5}$ for the regions in the YGP under each pattern. There was no obvious correlation between the average values of $PM_{2.5}$ and the strength of low pressure of the four patterns. The reason was that the intensity of the emission source was also one of the important factors of pollution in addition to the meteorological conditions. However, there was significant regional feature (SW > SE > NE > NW), which suggested the influence of the meteorological conditions of the transportation. Horizontal winds at 800 hPa also illustrated the two transport pathways from the ICP to the YGP, with one from northern Myanmar to western YGP and the other from the adjacent areas of Myanmar, Laos, and Vietnam to the YGP.

Figure 9 shows the zonal vertical circulation along latitude 24.5°N for each of the four weather patterns. All patterns showed significant downward and upward movements from the surface to 700–750 hPa (3.0–3.5 km) west of the plateau (longitude of 93°–98°E), especially at ~95°E (western Myanmar) and ~98°E (the western border of the plateau). Such air disturbances provided favorable conditions for aerosol uplift but showed weakening tendencies from Pattern 1 to Pattern 4. The zonal wind field showed westerlies at an altitude of 500–800 hPa, which was an important driver of the eastward transport of uplifted aerosols to the YGP. Therefore, both the vertical wind disturbance and zonal westerly flows were conducive to the uplift of smoke from Myanmar and the eastward transport to the western YGP region, especially for Pattern 1. The meridional winds in the western and central parts of the plateau were mostly southerly but small.

The meridional vertical circulation showed weak updrafts around 20–22°N (Figure 10). The strong meridional southerly airflows provided favorable conditions for aerosol climbing from eastern Myanmar and northern Laos/Vietnam to the south and center of the YGP. In addition, the zonal airflows were almost westerly from 18° to 28°N below 500 hPa, promoting eastward transport of smoke to the YGP. The vertical velocities in Patterns 4 and 3 were larger than those in Patterns 1 and 2, indicating a stronger uplift from the adjacent areas of Myanmar, Laos, and Vietnam to the YGP.

In summary, our work revealed two typical pathways of smoke transport from the ICP to the YGP. One pathway was from northern Myanmar to the western part of the YGP, another was from eastern Myanmar and north Laos/Vietnam to the YGP. These pathways are consistent with previous findings based on 1–2 cases of smoke transport (Fu et al., 2012; Li et al., 2017b; Xing et al., 2021). Moreover, Pattern 1, with the lowest pressure

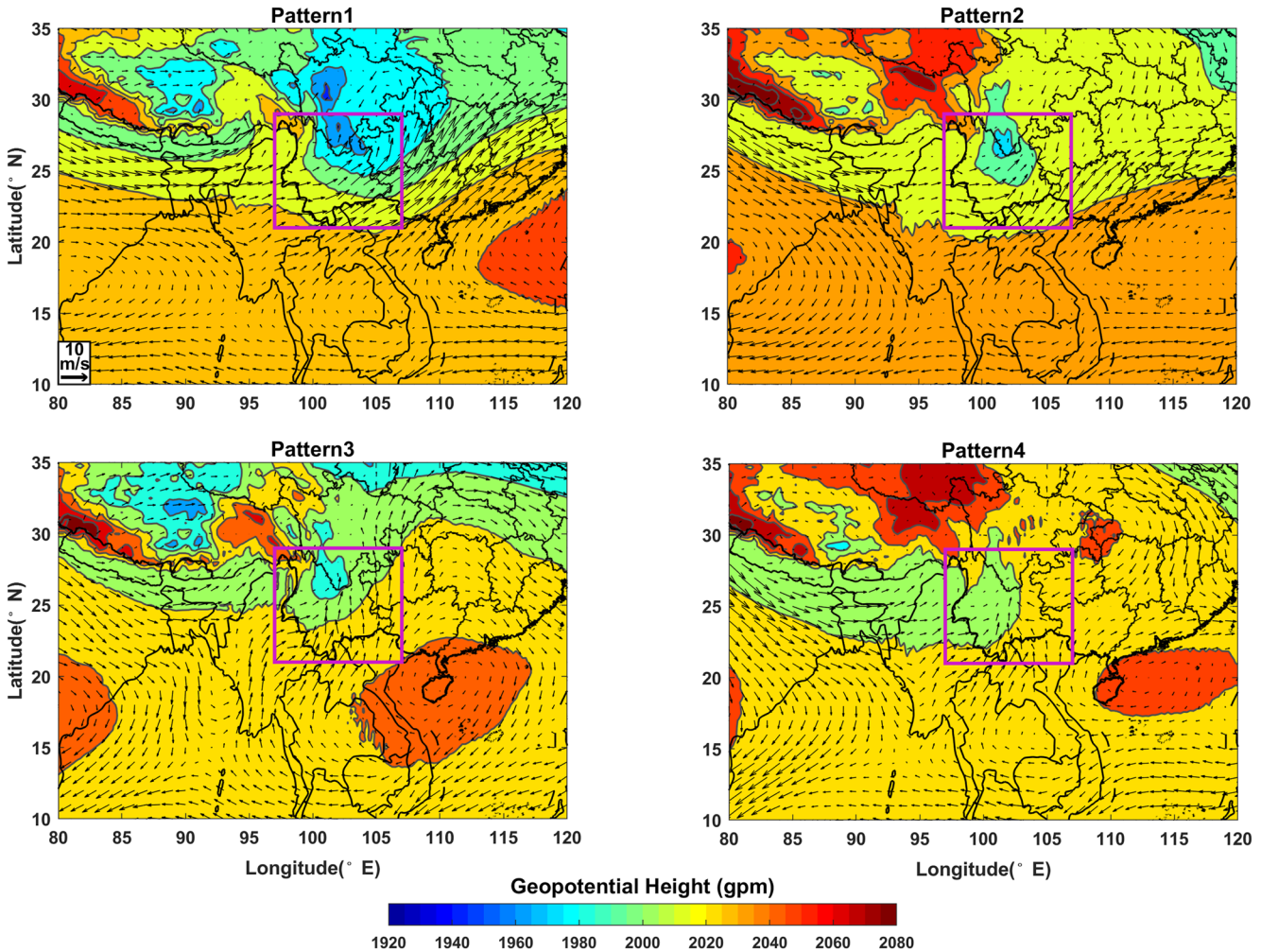

Figure 8. The ERA5 mean geopotential height (gpm) overlaid with horizontal winds (m/s) at 800 hPa under each of the four weather patterns on regional polluted days during March–April from 2015 to 2019. The pink box in figure is the domain of classification.

over northern/eastern YGP and the strongest zonal vertical wind disturbance, was the weather pattern that was most favorable for smoke transport through the first pathway. Pattern 4, with low pressure located at western/central YGP and the strongest meridional southerly airflows, was the weather pattern which was more likely to promote smoke aerosols transport through the second pathway. Pattern 2 and 3 transported smoke through the two pathways.

Table 1
The Statistic of the Mean Concentrations of $PM_{2.5}$ ($\mu g\ m^{-3}$) for the Regions in the YGP Under Each Pattern

Region	Pattern 1	Pattern 2	Pattern 3	Pattern 4	Average
SW	72.02	77.94	74.86	82.44	76.82
SE	60.90	66.93	44.15	58.93	57.73
NE	44.25	42.35	45.84	44.14	44.15
NW	34.46	37.52	39.42	42.86	38.57
Average	66.46	72.44	59.51	70.69	-

Note. YGP, Yungui Plateau.

4. Conclusions

Using ground-based monitoring data, ERA5 reanalysis of meteorology, and GEOS-Chem simulations, the impacts of biomass burning on vertical $PM_{2.5}$ over the YGP and the potential transport mechanisms of aerosols during the ICP fire seasons in 2015–2019 were analyzed. The main conclusions are as follows:

1. The average daily $PM_{2.5}$ concentration over the YGP was $36.06 \pm 14.86\ \mu g\ m^{-3}$ in March–April from 2015 to 2019. The regional mean $PM_{2.5}$ concentration decreased gradually from the south to the north. The SW region suffered the most days of pollution with the highest $PM_{2.5}$ concentration of $53.77\ \mu g\ m^{-3}$ at Xishuangbanna Station.

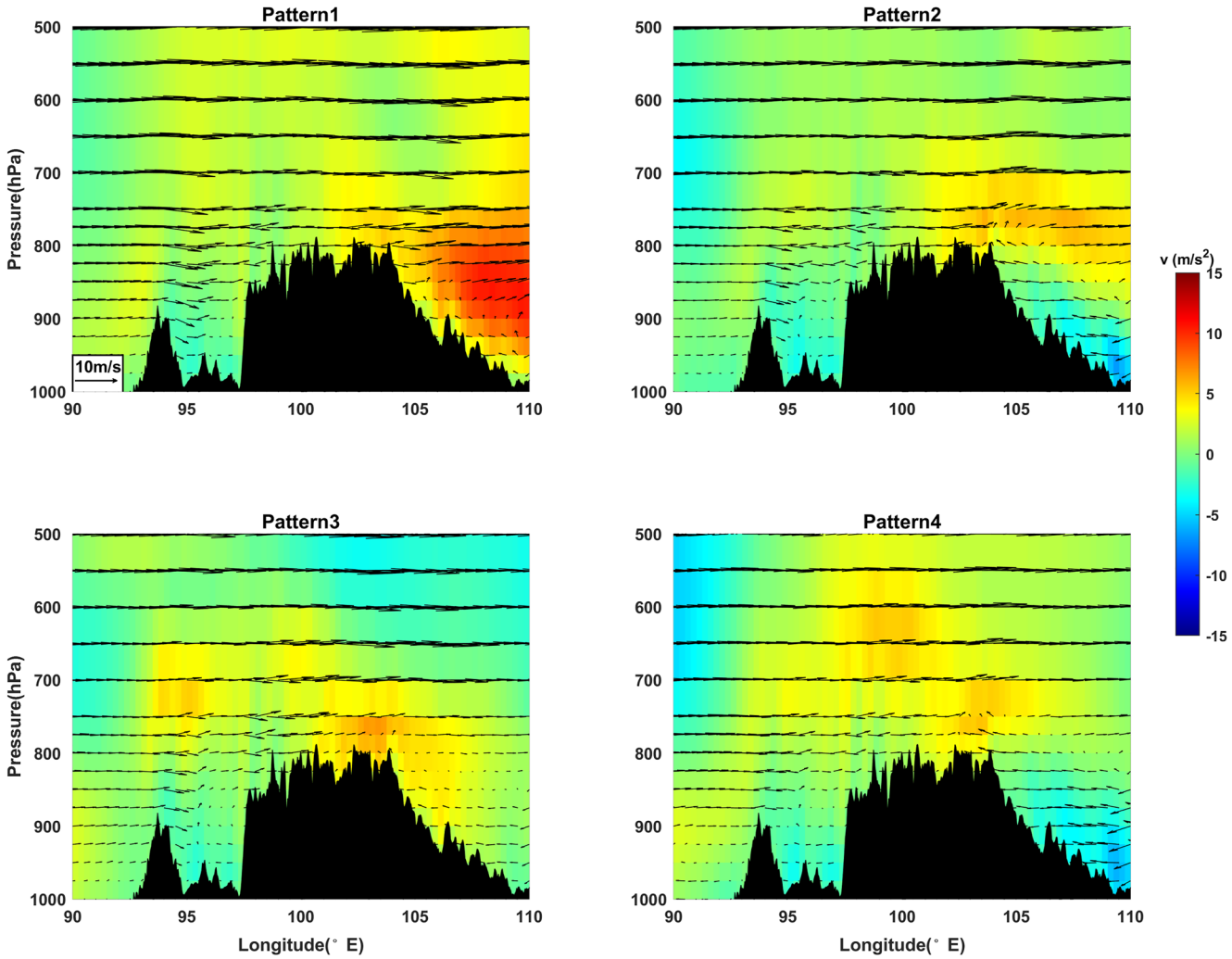

Figure 9. The ERA5 zonal vertical wind vectors (zonal wind and 100 times vertical velocity) and meridional wind (filled with color) along the latitude of 24.5°N under each of the four weather patterns. The black shaded area represents the terrain.

2. The GEOS-Chem model reasonably captured the observed spatiotemporal $PM_{2.5}$ concentrations over the YGP. The model simulations showed that fire aerosols could be uplifted to a height of 3–4 km and contribute approximately 50% of the vertical $PM_{2.5}$ from west to east of the YGP. This contribution is even higher at 60% for the vertical $PM_{2.5}$ from south to north of the YGP.
3. Four weather patterns were identified on regional polluted days over the YGP. One pattern (Pattern 1) with the lowest pressure over northern/eastern YGP and the strongest zonal vertical wind disturbance was the most favorable for smoke eastward transport from Myanmar to the western part of the YGP. Another pattern (Pattern 4) with low pressure located at the western/central YGP and the strongest meridional southerly airflows was more beneficial to smoke aerosols transported from eastern Myanmar and northern Laos/Vietnam to the YGP.

This work revealed the large contributions of fire emissions to the vertical $PM_{2.5}$ concentrations over the YGP during the fire season of the neighboring ICP region. This improved understanding of the environmental effects of smoke aerosols. The analyses of meteorological conditions deepened understanding of the smoke transport mechanisms between special terrains. Moreover, the classification of weather pattern on regional polluted days could provide some help for the forecasting of pollution events over the YGP.

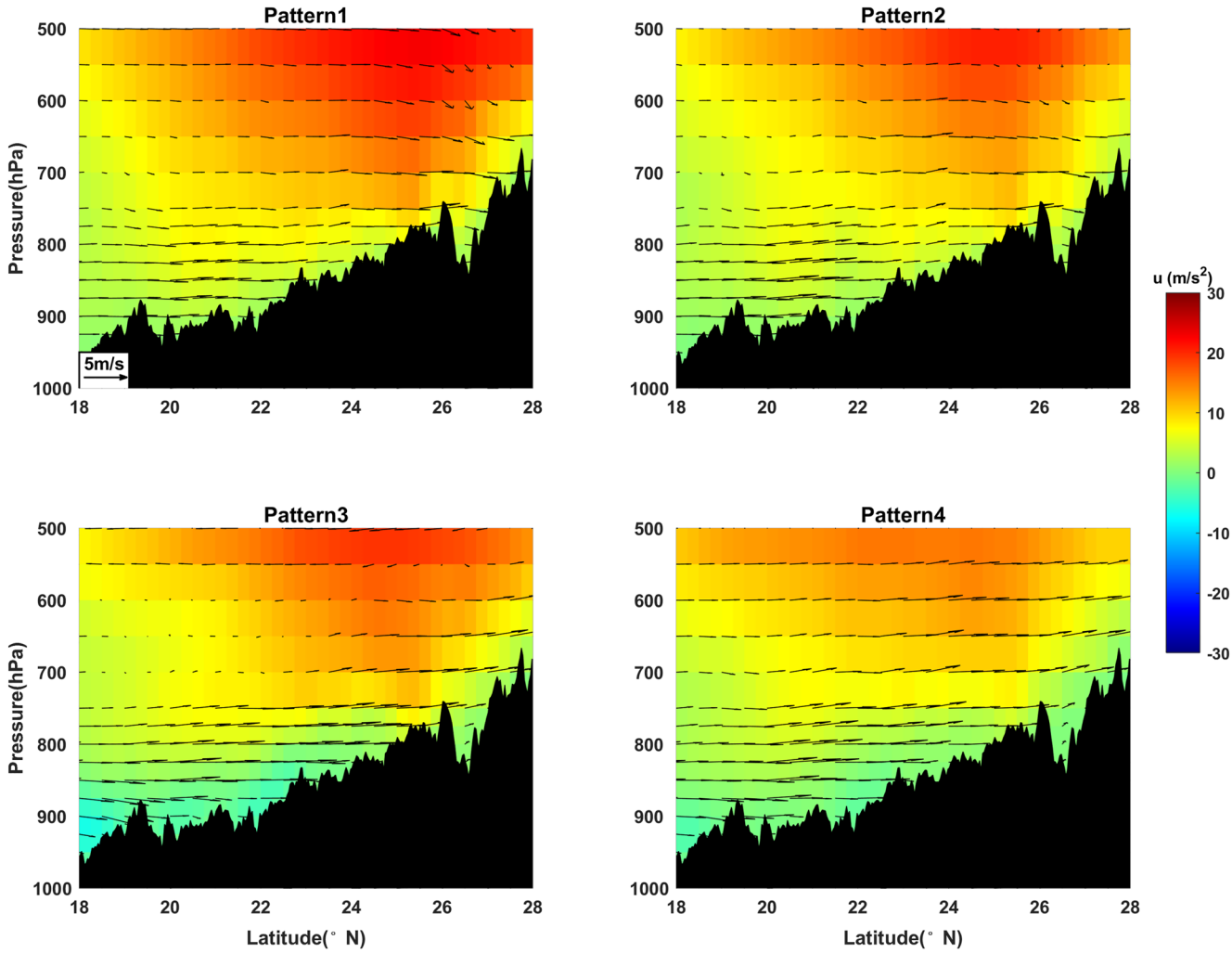

Figure 10. The ERA5 meridional vertical wind vectors (meridional wind and 100 times vertical velocity) and zonal wind (filled with color) along the longitude of 101.25°E under each of the four weather patterns. The black shaded area represents the terrain.

Conflict of Interest

The authors declare no conflicts of interest relevant to this study.

Data Availability Statement

The hourly data of $PM_{2.5}$ at the 16 stations can be accessed at Zenodo (https://doi.org/10.5281/zenodo.6578905). The ERA5 data can be downloaded from https://cds.climate.copernicus.eu/. The GEOS-Chem model code and shared data, including GFED inventory, are available online (http://wiki.seas.harvard.edu/geos-chem/index.php/Main_Page).

Acknowledgments
This research was supported by the National Key Research and Development Program of China (2019YFC0214604), the National Science Fund for Distinguished Young Scholars (41825011), the National Natural Science Foundation of China (41975161,42030608,42030612), and the Natural Science Foundation of Jiangsu Province (BK20170943). JW's participation is made possible via in-kind support from the University of Iowa.

References

Akagi, S. K., Yokelson, R. J., Wiedinmyer, C., Alvarado, M. J., Reid, J. S., Karl, T., et al. (2011). Emission factors for open and domestic biomass burning for use in atmospheric models. *Atmospheric Chemistry and Physics*, *11*(9), 4039–4072. https://doi.org/10.5194/acp-11-4039-2011

Ansmann, A., Baars, H., Tesche, M., Müller, D., Althausen, D., Engelmann, R., et al. (2009). Dust and smoke transport from Africa to South America: Lidar profiling over Cape Verde and the Amazon rainforest. *Geophysical Research Letters*, *36*(11), 1840–1846. https://doi.org/10.1029/2009GL037923

Arthur, D., & Vassilvitskii, S. (2006). k-means++: The advantages of careful seeding, Rep.

Bey, I., Jacob, D. J., Yantosca, R. M., Logan, J. A., Field, B. D., Fiore, A. M., et al. (2001). Global modeling of tropospheric chemistry with assimilated meteorology: Model description and evaluation. *Journal of Geophysical Research*, *106*(D19), 23073–23095. https://doi.org/10.1029/2001JD000807

Cheng, Z., Wang, S., Fu, X., Watson, J. G., Jiang, J., Fu, Q., et al. (2014). Impact of biomass burning on haze pollution in the Yangtze River delta, China: A case study in summer 2011. *Atmospheric Chemistry and Physics*, *14*(9), 4573–4585. https://doi.org/10.5194/acp-14-4573-2014

Dang, R., & Liao, H. (2019). Severe winter haze days in the Beijing–Tianjin–Hebei region from 1985 to 2017 and the roles of anthropogenic emissions and meteorology. *Atmospheric Chemistry and Physics*, *19*(16), 10801–10816. https://doi.org/10.5194/acp-19-10801-2019

Ding, K., Huang, X., Ding, A., Wang, M., Su, H., Kerminen, V. M., et al. (2021). Aerosol-boundary-layer-monsoon interactions amplify semi-direct effect of biomass smoke on low cloud formation in Southeast Asia. *Nature Communications*, *12*(1), 6416. https://doi.org/10.1038/s41467-021-26728-4

Dong, X., & Fu, J. S. (2015). Understanding interannual variations of biomass burning from Peninsular Southeast Asia, part II: Variability and different influences in lower and higher atmosphere levels. *Atmospheric Environment*, *115*, 9–18. https://doi.org/10.1016/j.atmosenv.2015.05.052

Engling, G., Zhang, Y. N., Chan, C. Y., Sang, X. F., Lin, M., Ho, K. F., et al. (2011). Characterization and sources of aerosol particles over the southeastern Tibetan Plateau during the Southeast Asia biomass-burning season. *Tellus B: Chemical and Physical Meteorology*, *63*(1), 117–128. https://doi.org/10.1111/j.1600-0889.2010.00512.x

Fu, J. S., Hsu, N. C., Gao, Y., Huang, K., Li, C., Lin, N. H., & Tsay, S. C. (2012). Evaluating the influences of biomass burning during 2006 BASE-ASIA: A regional chemical transport modeling. *Atmospheric Chemistry and Physics*, *12*(9), 3837–3855. https://doi.org/10.5194/acp-12-3837-2012

Giglio, L., Randerson, J. T., & van der Werf, G. R. (2013). Analysis of daily, monthly, and annual burned area using the fourth-generation global fire emissions database (GFED4). *Journal of Geophysical Research: Biogeosciences*, *118*, 317–328. https://doi.org/10.1002/jgrg.20042

Gong, C., & Liao, H. (2019). A typical weather pattern for ozone pollution events in North China. *Atmospheric Chemistry and Physics*, *19*(22), 13725–13740. https://doi.org/10.5194/acp-19-13725-2019

Hersbach, H., Bell, B., Berrisford, P., Hirahara, S., Horányi, A., Muñoz-Sabater, J., et al. (2020). The ERA5 global reanalysis. *The Quarterly Journal of the Royal Meteorological Society*, *146*(730), 1999–2049. https://doi.org/10.1002/qj.3803

Hoffmann, L., Günther, G., Li, D., Stein, O., Wu, X., Griessbach, S., et al. (2019). From ERA-Interim to ERA5: The considerable impact of ECMWF's next-generation reanalysis on Lagrangian transport simulations. *Atmospheric Chemistry and Physics*, *19*(5), 3097–3124. https://doi.org/10.5194/acp-19-3097-2019

Hu, J., Wang, Y., Ying, Q., & Zhang, H. (2014). Spatial and temporal variability of $PM_{2.5}$ and PM_{10} over the north China Plain and the Yangtze River delta, China. *Atmospheric Environment*, *95*, 598–609. https://doi.org/10.1016/j.atmosenv.2014.07.019

Huang, J., Minnis, P., Lin, B., Wang, T., Yi, Y., Hu, Y., et al. (2006). Possible influences of Asian dust aerosols on cloud properties and radiative forcing observed from MODIS and CERES. *Geophysical Research Letters*, *33*(6), L06824. https://doi.org/10.1029/2005gl024724

IPCC. (2013). *Climate change 2013: The physical science basis. Contribution of working group I to the fifth assessment report of the intergovernmental panel on climate change*. (pp. 1535). Cambridge University Press, https://doi.org/10.1017/CBO9781107415324

Keller, C. A., Long, M. S., Yantosca, R. M., Da Silva, A. M., Pawson, S., & Jacob, D. J. (2014). Hemco v1.0: A versatile, ESMF-compliant component for calculating emissions in atmospheric models. *Geoscientific Model Development Discussions*, *7*(1), 1115–1136. https://doi.org/10.5194/gmdd-7-1115-2014

Lei, Y., Yue, X., Liao, H., Gong, C., & Zhang, L. (2020). Implementation of Yale interactive terrestrial Biosphere model v1.0 into GEOS-Chem v12.0.0: A tool for biosphere–chemistry interactions. *Geoscientific Model Development*, *13*(3), 1137–1153. https://doi.org/10.5194/gmd-13-1137-2020

Li, C. C., Mao, J. T., Lau, A. K. H., Chen, J. C., Yuan, Z. B., Liu, X. Y., et al. (2003). Characteristics of distribution and seasonal variation of aerosol optical depth in eastern China with MODIS products. *Chinese Science Bulletin*, *48*, 2488–2495. https://doi.org/10.1360/03wd0224

Li, J., Lv, Q., Zhang, M., Wang, T., Kawamoto, K., Chen, S., & Zhang, B. (2017a). Effects of atmospheric dynamics and aerosols on the fraction of supercooled water clouds. *Atmospheric Chemistry and Physics*, *17*(3), 1847–1863. https://doi.org/10.5194/acp-17-1847-2017

Li, J., Zhang, Y., Wang, Z., Sun, Y., Fu, P., Yang, Y., et al. (2017b). Regional impact of biomass burning in Southeast Asia on atmospheric aerosols during the 2013 seven south-east Asian studies project. *Aerosol and Air Quality Research*, *17*(12), 2924–2941. https://doi.org/10.4209/aaqr.2016.09.0422

Li, M., Wang, L., Liu, J., Gao, W., Song, T., Sun, Y., et al. (2020). Exploring the regional pollution characteristics and meteorological formation mechanism of $PM_{2.5}$ in North China during 2013–2017. *Environment International*, *134*, 105283. https://doi.org/10.1016/j.envint.2019.105283

Li, M., Zhang, Q., Kurokawa, J. I., Woo, J. H., He, K., Lu, Z., et al. (2017c). MIX: A mosaic Asian anthropogenic emission inventory under the international collaboration framework of the MICS-Asia and HTAP. *Atmospheric Chemistry and Physics*, *17*(2), 935–963. https://doi.org/10.5194/acp-17-935-2017

Li, X., Cheng, T., Shi, S., Guo, H., Wu, Y., Lei, M., et al. (2021). Evaluating the impacts of burning biomass on $PM_{2.5}$ regional transport under various emission conditions. *Science of the Total Environment*, *793*, 148481. https://doi.org/10.1016/j.scitotenv.2021.148481

Li, Y., Liu, J., Han, H., Zhao, T., Zhang, X., Zhuang, B., et al. (2019). Collective impacts of biomass burning and synoptic weather on surface $PM_{2.5}$ and CO in Northeast China. *Atmospheric Environment*, *213*, 64–80. https://doi.org/10.1016/j.atmosenv.2019.05.062

Liang, X., Li, S., Zhang, S., Huang, H., & Chen, S. X. (2016). $PM_{2.5}$ data reliability, consistency, and air quality assessment in five Chinese cities. *Journal of Geophysical Research: Atmospheres*, *121*, 10220–210236. https://doi.org/10.1002/2016JD024877

Liang, Y., Gui, K., Zheng, Y., Yang, X., Li, X., Liu, C., et al. (2019). Impact of biomass burning in south and southeast Asia on background aerosol in Southwest China. *Aerosol and Air Quality Research*, *19*(5), 1188–1204. https://doi.org/10.4209/aaqr.2018.08.0324

Liao, T., Gui, K., Li, Y., Wang, X., & Sun, Y. (2021). Seasonal distribution and vertical structure of different types of aerosols in southwest China observed from CALIOP. *Atmospheric Environment*, *246*, 118145. https://doi.org/10.1016/j.atmosenv.2020.118145

Lin, J. T., & McElroy, M. B. (2010). Impacts of boundary layer mixing on pollutant vertical profiles in the lower troposphere: Implications to satellite remote sensing. *Atmospheric Environment*, *44*(14), 1726–1739. https://doi.org/10.1016/j.atmosenv.2010.02.009

Lin, S. J., & Rood, R. B. (1996). Multidimensional flux-form semi-Lagrangian transport schemes. *Monthly Weather Review*, *124*(9), 2046–2070. https://doi.org/10.1175/1520-0493(1996)

Liu, H., Jacob, D. J., Bey, I., & Yantosca, R. M. (2001). Constraints from 210Pb and 7Be on wet deposition and transport in a global three-dimensional chemical tracer model driven by assimilated meteorological fields. *Journal of Geophysical Research*, *106*(D11), 12109–12128. https://doi.org/10.1029/2000JD900839

Liu, Y., Huang, J., Shi, G., Takamura, T., Khatri, P., Bi, J., et al. (2011). Aerosol optical properties and radiative effect determined from sky-radiometer over Loess Plateau of Northwest China. *Atmospheric Chemistry and Physics*, *11*(22), 11455–11463. https://doi.org/10.5194/acp-11-11455-2011

Lloyd, S. (1982). Least squares quantization in PCM. *IEEE Transactions on Information Theory*, *28*(2), 129–137. https://doi.org/10.1109/TIT.1982.1056489

Luo, Y. X., Zheng, X. B., Zhao, T. L., & Chen, J. (2014). A climatology of aerosol optical depth over China from recent 10 years of MODIS remote sensing data. *International Journal of Climatology*, *34*(3), 863–870. https://doi.org/10.1002/joc.3728

Mielonen, T., Portin, H., Komppula, M., Leskinen, A., Tamminen, J., Ialongo, I., et al. (2012). Biomass burning aerosols observed in Eastern Finland during the Russian wildfires in summer 2010 – Part 2: Remote sensing. *Atmospheric Environment*, *47*, 279–287. https://doi.org/10.1016/j.atmosenv.2011.07.016

Ming, L., Jin, L., Li, J., Fu, P., Yang, W., Liu, D., et al. (2017). $PM_{2.5}$ in the Yangtze River Delta, China: Chemical compositions, seasonal variations, and regional pollution events. *Environmental Pollution*, *223*, 200–212. https://doi.org/10.1016/j.envpol.2017.01.013

Mu, M., Randerson, J. T., van der Werf, G. R., Giglio, L., Kasibhatla, P., Morton, D., et al. (2011). Daily and 3-hourly variability in global fire emissions and consequences for atmospheric model predictions of carbon monoxide. *Journal of Geophysical Research*, *116*, D24303. https://doi.org/10.1029/2011jd016245

Péré, J. C., Bessagnet, B., Mallet, M., Waquet, F., Chiapello, I., Minvielle, F., et al. (2014). Direct radiative effect of the Russian wildfires and its impact on air temperature and atmospheric dynamics during August 2010. *Atmospheric Chemistry and Physics*, *14*(4), 1999–2013. https://doi.org/10.5194/acp-14-1999-2014

Poulain, L., Fahlbusch, B., Spindler, G., Müller, K., van Pinxteren, D., Wu, Z., et al. (2021). Source apportionment and impact of long-range transport on carbonaceous aerosol particles in central Germany during HCCT-2010. *Atmospheric Chemistry and Physics*, *21*(5), 3667–3684. https://doi.org/10.5194/acp-21-3667-2021

Saide, P., Spak, S., Pierce, R., Otkin, J., Schaack, T., Heidinger, A., et al. (2015). Central American biomass burning smoke can increase tornado severity in the US. *Geophysical Research Letters*, *42*(3), 956–965. https://doi.org/10.1002/2014GL062826

Song, Y., Zhang, Y., Xie, S., Zeng, L., Zheng, M., Salmon, L. G., et al. (2006). Source apportionment of $PM_{2.5}$ in Beijing by positive matrix factorization. *Atmospheric Environment*, *40*(8), 1526–1537. https://doi.org/10.1016/j.atmosenv.2005.10.039

Stoerk, T. (2016). Statistical corruption in Beijing's air quality data has likely ended in 2012. *Atmospheric Environment*, *127*, 365–371. https://doi.org/10.1016/j.atmosenv.2015.12.055

Streets, D. G., Yarber, K. F., Woo, J. H., & Carmichael, G. R. (2003). Biomass burning in Asia: Annual and seasonal estimates and atmospheric emissions. *Global Biogeochemical Cycles*, *17*(4), 1759–1768. https://doi.org/10.1029/2003gb002040

Takemura, T., Nozawa, T., Emori, S., Nakajima, T. Y., & Nakajima, T. (2005). Simulation of climate response to aerosol direct and indirect effects with aerosol transport-radiation model. *Journal of Geophysical Research*, *110*, D02202. https://doi.org/10.1029/2004jd005029

van der Werf, G. R., Randerson, J. T., Giglio, L., van Leeuwen, T. T., Chen, Y., Rogers, B. M., et al. (2017). Global fire emissions estimates during 1997–2016. *Earth System Science Data*, *9*(2), 697–720. https://doi.org/10.5194/essd-9-697-2017

Wang, J., & Christopher, S. A. (2006). Mesoscale modeling of central American smoke transport to the United States: 2. Smoke radiative impact on regional surface energy budget and boundary layer evolution. *Journal of Geophysical Research*, *111*, D14S92. https://doi.org/10.1029/2005jd006720

Wang, Q., Shao, M., Liu, Y., William, K., Paul, G., Li, X., et al. (2007). Impact of biomass burning on urban air quality estimated by organic tracers: Guangzhou and Beijing as cases. *Atmospheric Environment*, *41*(37), 8380–8390. https://doi.org/10.1016/j.atmosenv.2007.06.048

Wang, Q., Zhao, Z., Tian, J., Zhu, C., Ni, H., Zhang, Y., et al. (2017). Seasonal transport and dry deposition of black carbon aerosol in the Southeastern Tibetan Plateau. *Aerosol Science and Engineering*, *1*(4), 160–168. https://doi.org/10.1007/s41810-017-0016-y

Wang, S.-C., Wang, Y., Estes, M., Lei, R., Talbot, R., Zhu, L., & Hou, P. (2018). Transport of central American fire emissions to the U.S. Gulf Coast: Climatological pathways and impacts on ozone and $PM_{2.5}$. *Journal of Geophysical Research: Atmospheres*, *123*, 8344–8361. https://doi.org/10.1029/2018JD028684

Wang, T., Tang, J., Sun, M., Liu, X., Huang, Y., Huang, J., et al. (2021). Identifying a transport mechanism of dust aerosols over South Asia to the Tibetan Plateau: A case study. *Science of the Total Environment*, *758*, 143714. https://doi.org/10.1016/j.scitotenv.2020.143714

Wang, Y., Jacob, D. J., & Logan, J. A. (1998). Global simulation of tropospheric O_3 -NOx -hydrocarbon chemistry: 1. Model formulation. *Journal of Geophysical Research*, *103*(D9), 10713–10725. https://doi.org/10.1029/98JD00158

Wesely, M. L. (1989). Parameterization of surface resistances to gaseous dry deposition in regional-scale numerical-models. *Atmospheric Environment*, *23*(6), 1293–1304. https://doi.org/10.1016/0004-6981(89)90153-4

Williams, J. E., van Weele, M., van Velthoven, P. F. J., Scheele, M. P., Liousse, C., & van der Werf, G. R. (2012). The impact of uncertainties in African biomass burning emission estimates on modeling global air quality, long range transport and tropospheric chemical lifetimes. *Atmosphere*, *3*(1), 132–163. https://doi.org/10.3390/Atmos3010132

Wu, S. L., Mickley, L. J., Jacob, D. J., Logan, J. A., Yantosca, R. M., & Rind, D. (2007). Why are there large differences between models in global budgets of tropospheric ozone? *Journal of Geophysical Research*, *112*, D05302. https://doi.org/10.1029/2006jd007801

Xing, L., Bei, N., Guo, J., Wang, Q., Liu, S., Han, Y., et al. (2021). Impacts of biomass burning in peninsular Southeast Asia on $PM_{2.5}$ concentration and ozone formation in Southern China during springtime—A case study. *Journal of Geophysical Research: Atmospheres*, *126*, e2021JD034908. https://doi.org/10.1029/2021jd034908

Yan, H., Li, Q., Sun, C., Yuan, Y., & Li, D. (2013). Criterion for determining the onset and end of the rainy season in Southwest China. *Chinese Journal of Atmospheric Sciences*, *37*, 1111–1128. https://doi.org/10.3878/j.issn.1006-9895.2013.12118

Yang, R., Wang, J., Zhang, T., & He, S. (2017). Change in the relationship between the Australian summer monsoon circulation and boreal summer precipitation over Central China in the late 1990s. *Meteorology and Atmospheric Physics*, *131*(1), 105–113. https://doi.org/10.1007/s00703-017-0556-3

Zhang, B., Wang, Y., & Hao, J. (2015). Simulating aerosol–radiation–cloud feedbacks on meteorology and air quality over eastern China under severe haze conditionsin winter. *Atmospheric Chemistry and Physics*, *15*(5), 2387–2404. https://doi.org/10.5194/acp-15-2387-2015

Zhang, L., Gong, S., Padro, J., & Barrie, L. (2001). A size-segregated particle dry deposition scheme for an atmospheric aerosol module. *Atmospheric Environment*, *35*(3), 549–560. https://doi.org/10.1016/S1352-2310(00)00326-5

Zhang, N., Cao, J., Wang, Q., Huang, R., Zhu, C., Xiao, S., & Wang, L. (2018). Biomass burning influences determination based on $PM_{2.5}$ chemical composition combined with fire counts at southeastern Tibetan Plateau during pre-monsoon period. *Atmospheric Research*, *206*, 108–116. https://doi.org/10.1016/j.atmosres.2018.02.018

Zhang, Q., Zheng, Y., Tong, D., Shao, M., Wang, S., Zhang, Y., et al. (2019). Drivers of improved $PM_{2.5}$ air quality in China from 2013 to 2017. *Proceedings of the National Academy of Sciences*, *116*(49), 24463–24469. https://doi.org/10.1073/pnas.1907956116

Zhang, Y.-L., & Cao, F. (2015). Fine particulate matter ($PM_{2.5}$) in China at a city level. *Scientific Reports*, *5*, 14884. https://doi.org/10.1038/srep14884

Zhou, Y., Xing, X., Lang, J., Chen, D., Cheng, S., Wei, L., et al. (2017). A comprehensive biomass burning emission inventory with high spatial and temporal resolution in China. *Atmospheric Chemistry and Physics*, *17*(4), 2839–2864. https://doi.org/10.5194/acp-17-2839-2017

Zhu, J., Xia, X., Che, H., Wang, J., Cong, Z., Zhao, T., et al. (2019). Spatiotemporal variation of aerosol and potential long-range transport impact over the Tibetan Plateau, China. *Atmospheric Chemistry and Physics*, *19*(23), 14637–14656. https://doi.org/10.5194/acp-19-14637-2019

Zhu, J., Xia, X., Wang, J., Zhang, J., Wiedinmyer, C., Fisher, J. A., & Keller, C. A. (2017). Impact of Southeast Asian smoke on aerosol properties in Southwest China: First comparison of model simulations with satellite and ground observations. *Journal of Geophysical Research: Atmospheres*, *122*, 3904–3919. https://doi.org/10.1002/2016JD025793